Magnetic and orbital order in $LaMnO_3$ under uniaxial strain: A model study

B. R. K. Nanda and S. Satpathy
Department of Physics, University of Missouri, Columbia, Missouri 65211, USA

(Received 4 November 2009; revised manuscript received 12 March 2010; published 25 May 2010)

The effect of uniaxial strain on electronic structure and magnetism in $LaMnO_3$ is studied from a model Hamiltonian that illustrates the competition between the Jahn-Teller, superexchange, and double-exchange interactions. We retain in our model the three main octahedral distortions (Q_1, Q_2, and Q_3), which couple to the Mn (e_g) electrons. Our results show the ground state to be a type A antiferromagnetic (AFM) insulating state for the unstrained case, consistent with experiments. With tensile strain (stretching along the c axis), the ground state changes into a ferromagnetic and eventually into a type G′ AFM structure, while with compressive strain, we find the type A switching into a type G structure. The orbital ordering, which displays the well-known checkerboard x^2-1/y^2-1 structure for the unstrained case, retains more or less the same character for compressive strain, while changing into the z^2-1 character for tensile strains. While Q_1 and Q_3 are fixed by the strain components ε_{xx} and ε_{zz} in our model, the magnitude of the in-plane distortion mode (Q_2), which varies to minimize the total energy, slowly diminishes with tensile strain, completely disappearing as the FM state is entered. Within our model, the FM state is metallic, while the three AFM states are insulating.

DOI: 10.1103/PhysRevB.81.174423 PACS number(s): 75.47.Lx, 75.10.−b, 71.70.Ej

I. INTRODUCTION

It is well known that the interplay between the orbital, lattice, and spin degrees of freedom in the lanthanum manganite, a key member of the colossal magnetoresistive materials, produces a checkerboard orbital-ordered ground state by the cooperative Jahn-Teller (JT) effect and simultaneously the type A antiferromagnetic ordering. However, a detail knowledge of what happens to this ground state under the application of strain or uniform pressure is lacking.

On the other hand, high-quality, lattice-matched heterostructures of the manganites have begun to be grown and studied, heterostructures that are frequently under uniaxial strain due to the pseudomorphic growth condition during epitaxial growth. The variation in layer thickness and substrate induces different magnetic ground states ranging from complete ferromagnetic ordering to a canted magnetic state or an antiferromagnetic state.[1–5] An interesting two-dimensional spin-polarized electron gas was also predicted for the manganite heterostructures.[6] In addition, the magnetotransport studies on bulk $LaMnO_3$ (LMO) under pressure[7–10] and LMO thin films grown on different substrates[11–17] show metal-insulator transitions accompanied by magnetic transitions. Theoretically, it is known that strain can change orbital ordering in LMO, which affects magnetism[18] and leads to modified properties in the manganite superlattices.[19,20] The commonalities involved in these are strain, either induced by pressure or due to substrate.

It is therefore important to understand the ground state of the underlying material, viz., the bulk LMO under uniaxial strain condition. It is the goal of the paper to provide this insight by studying a simple model Hamiltonian that contains the relevant interactions important for this material.

Density-functional studies[21–24] of the unstrained LMO have provided important insights into the physics of the system regarding how the JT coupling, orbital ordering, and magnetism are intertwined. The few such studies performed for the strained LMO are focused on the uniform pressure situation and indeed they do find changes in the magnitude of the JT distortions as well as in the conduction properties.[25,26] Above the critical pressure of 32 GPa, LMO becomes metallic and the JT distortion appears to be completely suppressed.[8,9] Systematic experimental work as well as theory work on the uniaxial strain situation is missing; yet, as already mentioned, this strain condition is frequently realized in thin films and superlattices grown on different substrates and must be understood before an understanding of the superlattices of LMO can be accomplished.

In this paper, we study the interplay between the lattice, orbital, and magnetic degrees of freedom in LMO under uniaxial strain condition by using a tight-binding model that

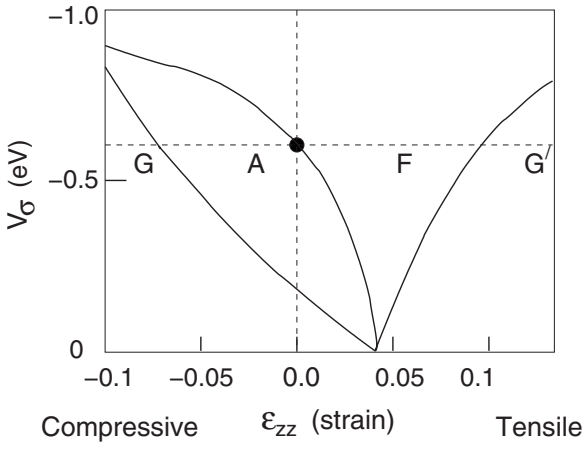

FIG. 1. The ground-state magnetic phase diagram for LMO as a function of strain and the $dd\sigma$ electronic hopping, V_σ, as obtained from our model. Type A represents the phase with ferromagnetic ab planes stacked antiferromagnetically along the c axis, while F and G stand, respectively, for the ferromagnetic and the Néel ordered antiferromagnetic state. We distinguish between two types of G states (G and G′) depending on the orbital occupancy of the Mn e_g electron: x^2-1 or y^2-1 for G and z^2-1 for G′. For LMO, V_σ is about −0.6 eV.

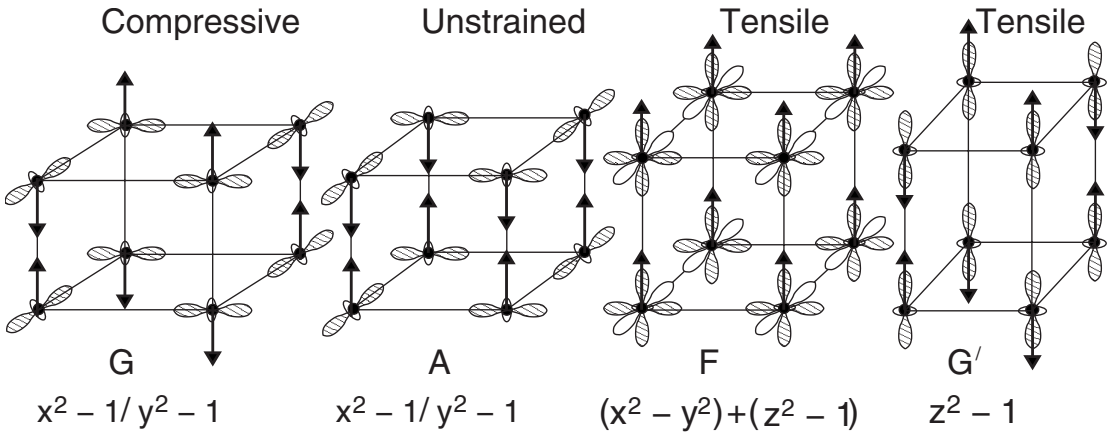

FIG. 2. The magnetic and orbital order of the four phases under varying strain conditions as obtained from our model. Shown are only the Mn atoms and arrows denote the t_{2g} core spins. Tensile strain means stretching along the c direction, normal to the ab plane.

includes the relevant interactions, viz., the antiferromagnetic superexchange between the t_{2g} core spins, the double exchange between the core spins and the itinerant e_g electrons, the electronic band-structure energy, the Coulomb interaction, as well as the JT coupling between the e_g electrons and the lattice.

At this stage, a model study is more instructional than a density-functional study, since unlike the latter, one can vary here the relative strengths of the various interactions and study their effect on the ground state, providing us with valuable insight into the system. This study will be important in understanding the experimental results on strained LMO as well as help interpret results of detail *ab initio* calculations, which are in progress and will be reported elsewhere.[27]

Our results, summarized in Figs. 1 and 2, show that the magnetic state, the JT distortions, the orbital ordering, as well as conduction properties, all change with uniaxial strain. As strain changes from compressive to tensile, the system changes from a type G antiferromagnetic (AFM) to the type A AFM phase, then to a ferromagnetic phase (F), ultimately changing into a type G′ phase. The FM phase is metallic, while the rest are insulating phases. As regards the orbital ordering, while the unstrained LMO shows the well-known checkerboard x^2-1/y^2-1 ordering on the ab plane, the application of compressive strain retains the same orbital structure more or less, while tensile strain results in a z^2-1 orbital ordering. As the strain is changed from compressive to tensile, the magnitude of the in-plane distortion (Q_2 mode) diminishes, eventually disappearing completely for the ferromagnetic phase and beyond. The changes in the various features are intertwined with one another as discussed below.

II. MODEL HAMILTONIAN

We consider the following model Hamiltonian, restricted to the Mn sites in a tetragonal lattice, with lattice constants being different along the plane and normal to the plane in order to accommodate the uniaxial strain

$$\mathcal{H} = \sum_i \frac{1}{2} K Q_i^2 + \sum_i \mathcal{H}_{\mathrm{JT}}^i + \mathcal{H}_{ke} + \mathcal{H}_U + \frac{J}{2} \sum_{\langle ij \rangle} \vec{S}_i \cdot \vec{S}_j, \quad (1)$$

where i is the site index and $\langle ij \rangle$ denotes summation over nearest-neighbor (NN) sites. The last term describes the antiferromagnetic superexchange interaction between the Mn t_{2g} spins, treated as classical, which provide the background for the motion of the itinerant Mn e_g electrons. The first two terms in the Hamiltonian describe the Jahn-Teller interaction of the Mn e_g electrons with the lattice, where the first term is the elastic energy with $Q^2=Q_1^2+Q_2^2+Q_3^2$, with Q_1 being the breathing mode, Q_2 being the basal plane distortion mode, and Q_3 being the octahedral stretching mode as shown in Fig. 3. These are the three important modes that couple to the e_g electrons.

The JT interaction at each Mn site is given by[28]

$$\mathcal{H}_{\mathrm{JT}} = g' Q_1 I - g(Q_3 \tau_z + Q_2 \tau_x) - G(Q_3^2 - Q_2^2)\tau_z + 2GQ_2Q_3\tau_x, \quad (2)$$

where both linear and quadratic vibronic couplings are included. The quadratic coupling is necessary to describe the checkerboard orbital ordering on the ab plane.[29] In Eq. (2), $\vec{\tau}$ is the pseudospin describing the two e_g orbitals, viz., $|\uparrow\rangle = |z^2-1\rangle$ and $|\downarrow\rangle = |x^2-y^2\rangle$. Denoting the creation operators for these two orbitals on the ith site by $c_{i1}^\dagger$ and $c_{i2}^\dagger$, respectively, the pseudospin operator at the ith site in Eq. (2) is written as: $\vec{\tau}_i = \Sigma_{\alpha\beta} c_{i\alpha}^\dagger \vec{\tau}_{\alpha\beta} c_{i\beta}$, where the Greek indices denote the orbitals and i is the site index. The lattice interactions do not depend on the electron spin, which therefore does not

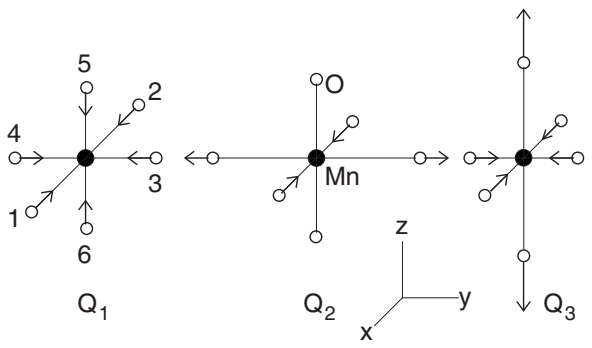

FIG. 3. Vibronic modes for the MnO_6 octahedron with the eigenvectors: $|Q_1\rangle = (-X_1+X_2-Y_3+Y_4-Z_5+Z_6)/\sqrt{6}$, $|Q_2\rangle = (-X_1+X_2+Y_3-Y_4)/2$, and $|Q_3\rangle = (-X_1+X_2-Y_3+Y_4+2Z_5-2Z_6)/\sqrt{12}$, where X_1 denotes the x coordinate of the first oxygen atom, etc.

appear in Eq. (2). There is also an interoctahedral elastic energy term $K'\Sigma_{\langle ij\rangle_\alpha}\tilde{Q}_{i\alpha}\tilde{Q}_{j\alpha}$, where $\tilde{Q}_x \equiv (Q_3+\sqrt{3}Q_2)/2$, $\tilde{Q}_y \equiv (Q_3-\sqrt{3}Q_2)/2$, $\tilde{Q}_z \equiv Q_3$, and $\langle ij\rangle_\alpha$ denote the NN pairs of octahedra along the direction $\alpha=\hat{x}$, $\hat{y}$, or $\hat{z}$. This term leads to a checkerboard distortion on the *ab* plane of the type (Q_2,Q_3) alternating with $(-Q_2,Q_3)$ as discussed in detail in an earlier paper.[29] In this work, for simplicity, the interoctahedral term is not considered explicitly, but its effect is implicitly taken into account by assuming the checkerboard distortion.

The kinetic-energy term in the Hamiltonian may be written as

$$\mathcal{H}_{ke} = \sum_{\langle ij\rangle,\alpha\beta} t_{i\alpha,j\beta}\cos(\theta_{ij}/2)c^\dagger_{i\alpha}c_{j\beta} + \text{H.c.}, \tag{3}$$

where the value of the Hund's energy is taken as $J_H=\infty$. In this limit, the coupling between the core and the itinerant spins, $\mathcal{H}_{Hund}=-J_H\Sigma_{i\alpha}\vec{S}_i\cdot\vec{s}_{i\alpha}$, makes the electron state with the spin antialigned with the t_{2g} core spin at that site inaccessible to the system (core t_{2g} spin and the electron spin at the *i*th site are denoted by $\vec{S}_i$ and $\vec{s}_i$, respectively). Thus the itinerant electrons are effectively described as spinless with only its spin state aligned parallel to the core spin at a particular site being accessible to the system. The electron hopping is diminished by the well-known Anderson-Hasegawa $\cos(\theta_{ij}/2)$ factor, where θ_{ij} is the angle between the core spins at the two sites.[30,31] The NN hopping integral t depends on the relative positions of the two Mn sites. For NN along the planar directions, we have[32]

$$t_{\alpha\beta} = \begin{pmatrix} 1 & \mp\sqrt{3} \\ \mp\sqrt{3} & 3 \end{pmatrix}\frac{V_\sigma}{4}, \tag{4}$$

where the $\mp$ signs are for hopping along $\hat{x}$ or $\hat{y}$, respectively, while along $\hat{z}$, we have $t_{\alpha\beta}=\delta_{\alpha1}\delta_{\beta1}V_\sigma$. Here V_σ is the $dd\sigma$ hopping parameter and we have neglected the much smaller $dd\delta$ interaction.

The Coulomb interaction term contains the repulsion between the two orbitals on the same site

$$\mathcal{H}_U = \sum_i U n_{i1}n_{i2}. \tag{5}$$

A. Method of calculation

The total energy was calculated by solving Hamiltonian (1) in the Hartree-Fock approximation and adding the energies of the occupied states in the Brillouin zone, corresponding to one e_g electron per Mn atom. We studied various strain conditions and magnetic configurations. Specifically, we considered the typical magnetic ordering of the core spins found in the manganites, viz., the A, C, G, and F types of magnetic states. Type C was always found to be of higher energy within our model. To accommodate these structures, the unit cell in the lattice consisted of four Mn atoms.

The Coulomb interaction term in Eq. (5) was treated in the Hartree-Fock approximation

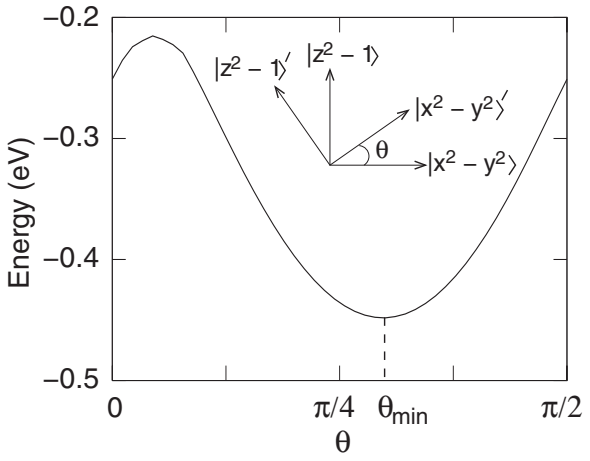

FIG. 4. Hartree-Fock energy as a function of the rotated basis set on a Mn atom for a typical case. Throughout this paper, we have always optimized θ in each case and for every Mn atom to obtain the best Hartree-Fock energy.

$$n_1n_2 = \langle n_1\rangle n_2 + \langle n_2\rangle n_1 - \langle c_1^\dagger c_2\rangle c_2^\dagger c_1 - \langle c_2^\dagger c_1\rangle c_1^\dagger c_2 - \langle n_1\rangle\langle n_2\rangle + \langle c_1^\dagger c_2\rangle\langle c_2^\dagger c_1\rangle, \tag{6}$$

where the first two terms are the direct term, the second two are the exchange term, and the final two terms correct for the double counting in the total energy. We find that the contribution of the exchange terms is relatively small. The Hartree-Fock approximation is not rotationally invariant for multiple-orbital basis set and the results depend on the choice of the basis within the same Hilbert space. Viewed another way, the fluctuations that are omitted, for instance, in the Hartree approximation, viz., $f_1f_2=(n_1-\langle n_1\rangle)(n_2-\langle n_2\rangle)$, can have different values depending on the choice of the orbital basis.

In view of the fact that the Hartree-Fock method has the strength of the variational principle, the best Hartree-Fock solution is the one where the total energy is minimized as a function of this choice of the basis set. For the two-dimensional Hilbert space of the e_g orbitals on each atom, the choice of the basis set is parameterized by the rotation angle θ. In each of our calculation, we have minimized the total energy as a function of this angle. A typical result of this angle dependence of the Hartree-Fock energy is shown in Fig. 4.

The results of Fig. 4 are easy to understand. The Jahn-Teller interaction on the atom shown results in the $|x^2-1\rangle$ being occupied, while the $|y^2-z^2\rangle$ orbital is empty. So, in this basis, which corresponds to the basis set rotation $\theta=\pi/3$, the mean-field Coulomb energy is zero, while in the unrotated basis set, both orbitals are partially occupied resulting in the energy $Un_1n_2=U\cos^2\theta\sin^2\theta=3U/16$. Intersite hopping changes this result somewhat, but not enough to change the overall features of Fig. 4.

B. Hamiltonian parameters

The typical values of the Hamiltonian parameters used in our calculations throughout, unless otherwise stated, are: $K=9$ eV/Å^2 following from the optical studies on

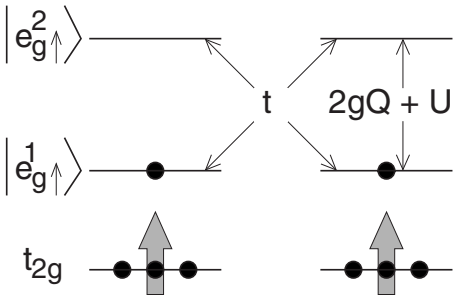

FIG. 5. Mn e_g level splitting due to the Jahn-Teller and Coulomb interactions. All other parameters remaining unchanged, a Coulomb U diminishes the strength of the ferromagnetic Anderson-Hasegawa double-exchange gain of energy, which is here equal to $-t^2/\Delta$, from the second-order perturbation theory with $\Delta=2gQ+U$.

$La_{0.85}Sr_{0.15}MnO_3$,[33] $g=1.5$ eV/Å, $G=1.5$ eV/Å^2, and $V_\sigma=-0.6$ eV guided by our earlier density-functional results.[29] The value of the exchange energy is taken as $J=30$ meV, which is close to the experimental value for $CaMnO_3$,[34,35] which has the $t_{2g}^3 e_g^0$ electronic configuration. Note that in our model Hamiltonian, g' is an unimportant parameter, as it affects the energies of both the e_g orbitals equally and therefore adds a constant to the total energy. The magnitude of the Coulomb parameter was taken as $U=2$ eV consistent with the argument that this parameter should be small for the e_g electrons.[36]

We should mention here that many effects of the on-site Coulomb term are diminished due to the presence of the JT coupling term in this system, as both the parameters lift the energy of the unoccupied e_g orbital with respect to the occupied one on the Mn atom. For instance, the phase boundaries of the orbitally ordered state were found to be remarkably the same, even at a quantitative level, whether one includes the Coulomb interaction or not, provided one increases the strength of the JT interaction to compensate for the lack of a Coulomb term.[37] We find a very similar result, viz., that the phase diagram and all essential physics discussed here remain the same whether or not we incorporate an on-site U in our model. Lack of a Coulomb U is again to be compensated by a larger JT coupling strength g. The essential point is illustrated in Fig. 5

In our second set of calculations, we have omitted U and instead changed the other parameters to $g=2.5$ eV/Å, $V_\sigma=-0.5$ eV, and $J=26$ meV. The first parameter was increased to compensate for the lack of the Coulomb term, while the small changes in the other two parameters were necessary to reproduce the type A structure to be the ground state as observed in the experiments. In two of the figures (Figs. 9 and 12), we have shown the results with the second set of parameters. The phase diagram for the case of $U=0$ is also very similar to Fig. 1.

C. Strain and the JT interaction

In our model, since we keep only the three main octahedral modes, the strain components are related to the magnitudes of the JT distortions. We consider only uniaxial strain conditions but no shear, so that only the diagonal components of the strain tensor are nonzero.

For the unstrained crystal, the ground state in our model has a tetragonal lattice structure with type A magnetic configuration and a checkerboard JT distortion and orbital ordering. This checkerboard JT distortion in our model results in a tetragonal structure with the lattice constants being $a=\sqrt{2/3}Q_{10}-Q_{30}/\sqrt{3}$ and $c=a+\sqrt{3}Q_{30}$, where the zero in the subscript denotes the calculated magnitudes for the unstrained LMO. The magnitudes of these distortions that minimize the ground-state energy clearly depend on the Hamiltonian parameters used in the model. For our typical parameters, we find that $Q_{20}\approx 0.18$ Å and $Q_{30}\approx -0.08$ Å, as compared to the experimental values of 0.28 Å and −0.10 Å, respectively.[38] Optimization of Q_1 for the Hamiltonian yields, trivially, the result that $Q_{10}=-g'/K$, while the cell volume is given by $a^2c\approx(\sqrt{2/3}Q_{10})^3$. So, in essence, the experimental volume of LMO, which corresponds to $Q_{10}=4.85$ Å determines the ratio of $-g'/K$.

We note that c and a are independent of the strength of the in-plane distortion Q_2. Therefore, any strain that changes c and a will directly affect the Q_1 and Q_3 distortions only, whereas the system will have an optimized Q_2 distortion in order to achieve the minimum in the ground-state energy. This is consistent with the experimental studies of bulk LMO under pressure, where it has been found that the Mn-O bond length along the c axis changes linearly with the lattice parameter of the LMO unit cell, while the Mn-O bond lengths along the plane follow a nonlinear behavior.[8,9]

Now, with uniaxial strain, the lengths of the axes become $a\ (1+\varepsilon_{xx})$ and $c\ (1+\varepsilon_{zz})$, respectively. The strain parameters completely determine the magnitudes of the breathing and the octahedral stretching modes, viz.,

$$Q_1 = Q_{10}(1 + 2\varepsilon_{xx}/3 + \varepsilon_{zz}/3),$$

$$Q_3 = Q_{30}(1 + \varepsilon_{zz}) + \sqrt{2}Q_{10}(\varepsilon_{zz} - \varepsilon_{xx})/3. \quad (7)$$

In addition, the Poisson's ratio ν relates the two strain components,[39] $\varepsilon_{xx}=(2\nu)^{-1}(\nu-1)\varepsilon_{zz}$, so that there is a single strain parameter ε_{zz} in the problem. Rewriting Eq. (7) in terms of this parameter, we have

$$Q_1 = Q_{10}\left(1 + \frac{2\nu-1}{3\nu}\varepsilon_{zz}\right),$$

$$Q_3 = Q_{30}(1 + \varepsilon_{zz}) + Q_{10}\frac{\sqrt{2}}{3}\frac{\nu+1}{2\nu}\varepsilon_{zz}, \quad (8)$$

so that in our model, the strain parameter fixes the values of the Q_1 and the Q_3 distortions. The magnetic configurations and the in-plane JT distortion Q_2 are then determined so as to minimize the total energy.

The value $\nu=1/2$ corresponds to conservation of volume under strain and the measured values for materials are not too far from this. For the manganites, the measured value is $\nu\approx 0.4$,[39,40] which we use in our calculations together with the unstrained distortions $Q_{10}=4.85$ Å and $Q_{30}=-0.08$ Å as indicated above. For the case of conserved volume ($\nu=1/2$), the value of Q_1 does not change with strain, while for

ν=0.4 and ε_{zz}=0.05, it changes by less than a percent from Q_{10}, while Q_3 changes significantly. Furthermore, because of the form of the Hamiltonian, Eqs. (1) and (2), Q_1 adds just an elastic energy and shifts the energies of both components of the e_g orbitals uniformly, irrespective of the magnetic structure of the Mn core spins, so that the relative energies of the different magnetic structures for a given strain ε_{zz} are not affected by Q_1. Thus in essence Q_3 remains the sole parameter in the problem for obtaining the ground states for different strains and the two parameters ε_{zz} and Q_3 can be used interchangeably to describe the strain condition. It has been recently shown that for manganites, the strain parameter ε_{zz} can be varied by as much as $\pm$0.05 by using different materials as substrates.[39]

III. RESULTS AND DISCUSSIONS

A. Isolated octahedra under strain

To begin on familiar grounds, we consider the situation where the intersite hopping integral V_σ=0 in Hamiltonian (1). This is equivalent to a collection of isolated MnO_6 JT centers, each under the applied strain condition. The octahedra interacts only via the superexchange interaction of the Mn core spins that results in the Néel AFM order, but the orbital occupancy and the JT distortions are determined by the interaction within a single octahedron. We see from Fig. 1 that in this case the magnetic ordering changes from type G AFM to type G′ AFM beyond a certain value of tensile strain. This can be easily understood as explained below.

The energy of an isolated octahedron, with one e_g electron occupied, is well known.[41] The expression is

$$E = \frac{1}{2}KQ^2 - Q[g^2 + G^2Q^2 + 2gG\cos(3\phi)]^{1/2}, \qquad (9)$$

where $Q=\sqrt{Q_2^2+Q_3^2}$ and $\phi=\tan^{-1}(Q_2/Q_3)$. This leads to the energy contours with three equivalent minima at $\phi=0, \pm 2\pi/3$ with $Q=g/(K-2G)$ and the corresponding occupied orbital as shown in Fig. 6.

Now, when the octahedron is placed in LMO, the strain parameter ε_{zz} fixes the magnitude of Q_3 as given by Eq. (8) with the result that the state of the octahedron is given by minimizing the energy with respect to Q_2 only. The constrained minima for a certain value of Q_3 are shown by the square dots in Fig. 6. For the isolated octahedron, there are two equivalent minima with either the x^2-1 or the y^2-1 occupation. In the solid, they become staggered resulting in the checkerboard orbital order in the *ab* plane. As strain is changed, Q_3 changes and the system traverses along the lines marked by the arrows in the figure. Beyond a certain tensile strain, the strength of the Q_2 mode sharply reduces to zero, which is also accompanied by a transition in the orbital occupancy from x^2-1 or y^2-1 to z^2-1. The octahedra interact only via the superexchange term when the hopping term V_σ is zero, so that the Néel order is retained throughout, resulting in the transition from type G to G′ configuration as the orbital state changes.

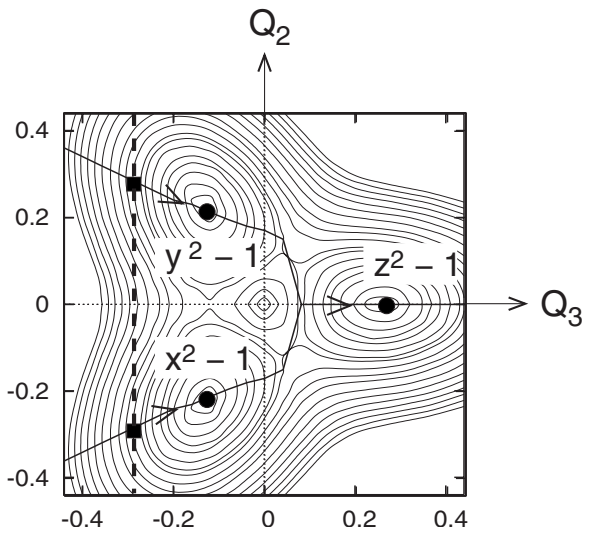

FIG. 6. Energy contours of an isolated Jahn-Teller center on the Q_2-Q_3 plane with linear and quadratic coupling. This figure corresponds to the G or G′ phase, since in these phases there is no hopping in our model. The three global minima are indicated by the circular dots along with the corresponding occupied orbital; one of the three minima is occupied in the isolated octahedron. For the octahedron in the solid, the strain parameter ε_{zz} fixes the magnitude of Q_3 and the octahedron occupies the state marked by the square dots. As Q_3 is changed, the system traverses along the lines marked by the arrows. Beyond a critical value of the tensile strain (i.e., a critical Q_3), the orbital order abruptly switches from x^2-1 or y^2-1 like to z^2-1, making thereby a transition from G to G′ state.

B. Interoctahedral hopping allowed

When the interoctahedral hopping is allowed ($V_\sigma \neq 0$), it leads to a cooperative JT ordering, i.e., that the JT distortions of the neighboring octahedra are organized so as to optimize the various energy terms in the solid. The ground-state configuration is determined by a competition between (i) the electron kinetic energy, which would prefer no JT distortion and a FM alignment of the core spins, so that all e_g orbitals are aligned and the kinetic energy gain due to hopping is maximized, (ii) the on-site JT interaction that would prefer a large octahedral distortion, at the same time balancing the elastic energy cost, and (iii) the superexchange energy that prefers antiferromagnetic alignment between all neighboring spins. If the electronic hopping is taken as zero, there is no conflict between the last two terms and a Néel state (G or G′) results as discussed above, simultaneously maximizing the JT energy gain and as well as the superexchange term.

With the switching on of the hopping term, all three energies cannot be simultaneously optimized. The resulting competition leads to a staggered orbital order accompanied by a staggered JT distortion, where both Q_2 and Q_3 distortions occur at each site with Q_2 changing sign on neighboring sites and the x^2-1 and y^2-1 orbitals alternately occupied. The system thus stabilizes in the orbital-ordered type A AFM state.[29]

When strain is applied, other magnetic phases compete, resulting in different ground-state structures as shown in Fig. 1. To gain insight into the possible phases in strained LMO,

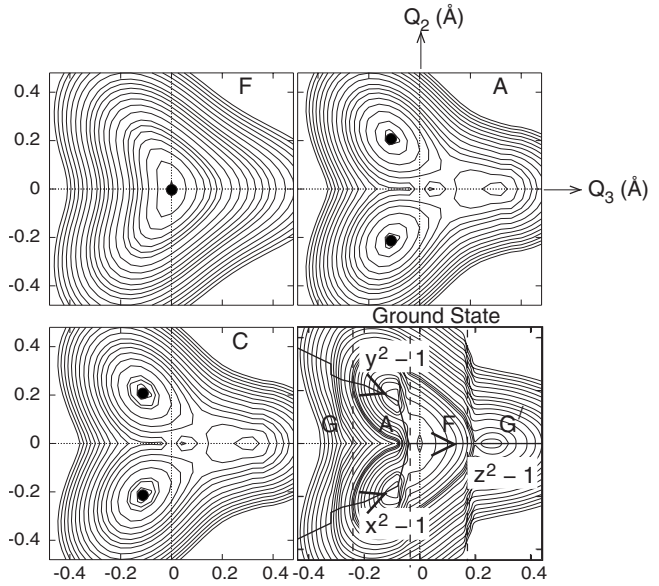

FIG. 7. Energy contours for different phases and for the minimum-energy phase (bottom right), which is synthesized from the first three contours here and from Fig. 6. For a fixed strain (fixed Q_3), the global minimum is obtained by varying Q_2 for each phase and comparing the minima thus obtained for each phase. The line with arrows indicates the state of the system as strain is varied. As strain changes from compressive to tensile, the magnetic state changes from $G \rightarrow A \rightarrow F \rightarrow G'$, the magnitude of Q_2 slowly diminishes eventually becoming zero and finally the orbital order changes from x^2-1/y^2-1 to z^2-1 type. Contours are obtained by solving Hamiltonian (1) and using the first set of parameters in Sec. II B.

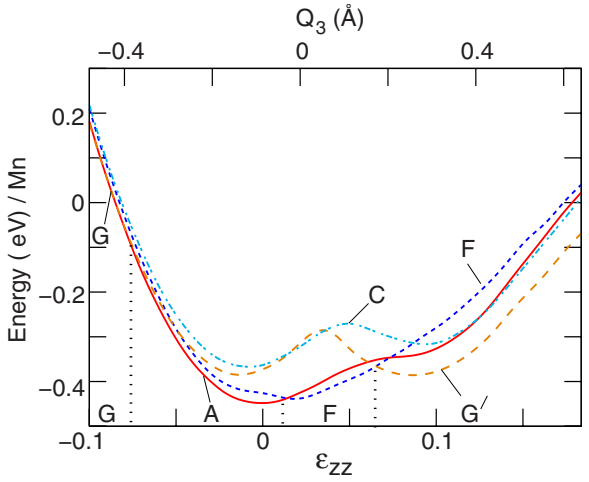

FIG. 8. (Color online) Total energy for the different phases as a function of strain. Parameters are the same as in Fig. 7.

we have kept the staggered JT distortion and examined four possible magnetic ordering, viz., A, F, G, and C. In Fig. 7 we have shown the energy contours in the Q_3-Q_2 plane for the type F, type A, and type C magnetic ordering. Results for type G ordering remain the same as in Fig. 6, irrespective of the magnitude of the hopping integral, since the Anderson-Hasegawa $\cos(\theta/2)$ factor makes the effective hopping to be zero anyway. For the ferromagnetic ordering, the e_g-e_g hopping is allowed in all the directions. It is the strongest when there is no JT splitting of the e_g orbitals. Therefore the global minimum for the ferromagnetic ordering occurs at the center of the Q_3-Q_2 plane as can seen from the energy contours of Fig. 7. As we deviate from the center, JT splitting reduces the effect of the hopping due to the energy denominator, which therefore weakens the FM stability.

For the type A AFM ordering, the e_g-e_g orbital hopping is forbidden along the c axis. Therefore, throughout the Q_3-Q_2 plane, the net gain in the band energy is weaker in comparison to the FM case. In this case, the competition between the JT energy and band energy leads to two global minima located at $Q_3 = -0.18$ Å and $Q_2 = \pm 0.32$ Å [see Fig. 7 (top right)] which is close to earlier experimental and theoretical studies.[8,22,29] In fact, taking the superexchange into account, these minima have the lowest energy in the Q_3-Q_2 plane when all the magnetic configurations are considered.

In the case of type C magnetic ordering, where the antiferromagnetic ab planes are stacked ferromagnetically along the c axis, the hopping between the z^2-1 orbitals along the c axis is only allowed and the remaining hopping interactions are forbidden either due to orbital symmetry along the c axis or due to the Anderson-Hasegawa $\cos(\theta/2)$ factor along the plane. As a result, the system gains very little band energy, making this phase unfavorable for all strains.

C. Total energy

The total energies of the various structures as a function of strain are plotted in Fig. 8. It is easy to understand several general features of the energy. First, note that with the energy minimum occurring at zero strain condition ($\varepsilon_{zz}=0$), the total energy is internally consistent. If the minimum occurred somewhere else, that would indicate that LMO would automatically occur with a different strain condition. The energy of the F structure does approach the minimum of the A structure at $\varepsilon_{zz}=0$, but does not come below it.

A second feature of the total energy is that for large strains, the octahedral distortion is strong, which leads to a large on-site splitting of the e_g states,

$$\epsilon_{\pm} = g' Q_1 \pm g\sqrt{Q_2^2 + Q_3^2} + U/2 \pm U/2, \qquad (10)$$

the lower orbital being fully occupied and the higher orbital empty. This, in turn, leads to a vanishing gain in energy due to hopping between the occupied and the unoccupied states because of the large energy denominator in the second-order perturbation theory, irrespective of the magnetic structure and the corresponding Anderson-Hasegawa $\cos(\theta/2)$ factors. The net result is that for large strains, the energies for all structures simply tend to a sum of the elastic energy and the on-site JT energy

$$E = (1/2)KQ^2 + g' Q_1 - g\sqrt{Q_2^2 + Q_3^2}. \qquad (11)$$

The quadratic dependence on the JT distortion or, equivalently, the strain for large strain for all magnetic structures is clearly seen in Fig. 8. The curves are parabolas with shifted minima for G and G′ structures, where the expression (11) is exact, since there is no hopping for these structures. For the remaining structures, there is a gain of energy due to hop-

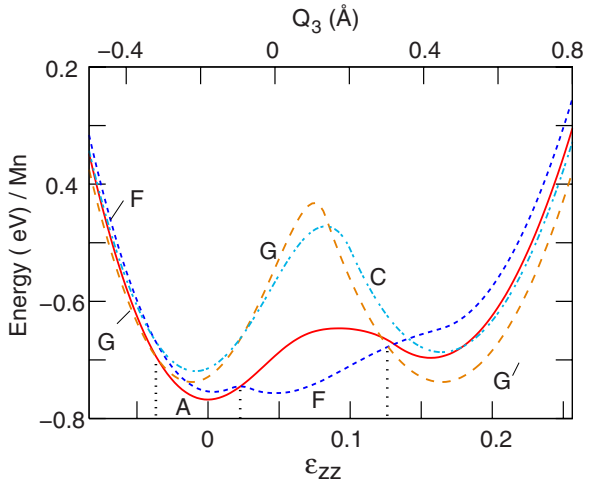

FIG. 9. (Color online) Same as Fig. 8, but with the second set of parameters with no Coulomb interaction and an enhanced Jahn-Teller term (see Sec. II B).

ping, being maximum for the ferromagnetic F structure, where hopping is allowed in all directions in the lattice. This leads to the stability of the F structure for small strain parameters as seen from the figure. The argument is consistent with the fact that the energy gain for small strain progressively increases from C to A to F (as seen in Fig. 8), where hopping is allowed along one, two, and three directions, respectively, for these structures.

Another point regarding the total energy of Fig. 8 is that the ferromagnetic phase is always close by in energy for small strain situations, which is suggestive of the reason why LMO thin films are usually observed to occur in the ferromagnetic phase, rather than the A phase of the bulk.

Finally, one might ask how is it possible that at larger strains the Néel ordered G or G′ state wins over the ferromagnetic F state. The reason is that as strain is increased, the progressively larger JT distortions split the e_g states more and more [Eq. (10)]. The kinetic-energy gain in the FM phase due to hopping between the occupied e_g state and the neighboring unoccupied e_g states progressively diminishes, due to the energy denominator in the second-order perturbation theory. This cannot overcome the superexchange energy cost, so that the Néel ordered states win in the limit of large strains.

Figure 9 shows the total energy of the various phases with the second set of parameters which had $U=0$ but a compensating larger JT parameter g. Both figures show similar energetics and the transition of phase $G \rightarrow A \rightarrow F \rightarrow G'$ as strain is changed. In fact, it is satisfying that density-functional band calculations show the same structural trend as a function of strain.[27] Notice that a comparison between Figs. 8 and 9 show that the energies of the various phases are closer to one another if the Coulomb U is taken into account. Indeed, energies of all phases would coincide in the limit $U \rightarrow \infty$, as there is no gain in energy from hopping since the unoccupied e_g orbitals are very high up in energy.

D. JT distortions and orbital occupancy

Turning now to the question of JT distortion strengths, Fig. 10 shows the variation in Q_2 and Q_3 modes and the

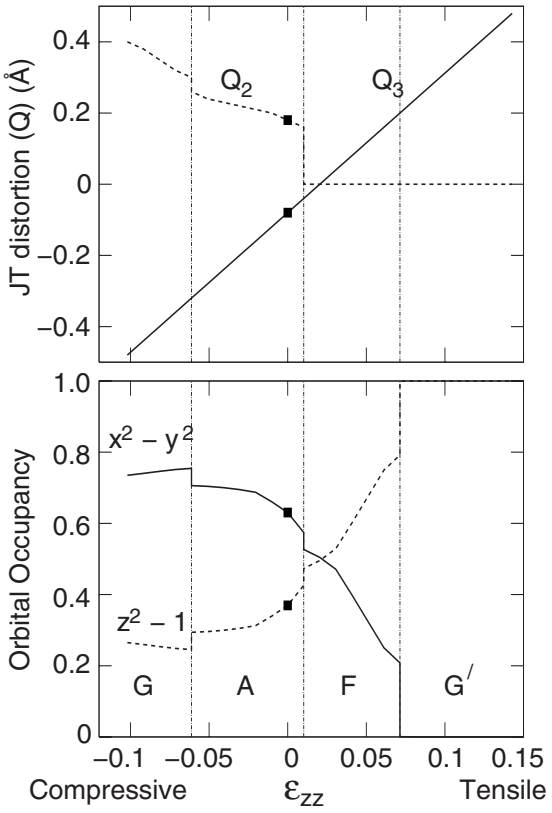

FIG. 10. Variation in the JT distortions (upper panel) and the occupancy of the Mn e_g orbitals (lower panel) as a function of the applied strain. In our model, Q_3 and ε_{zz} are linearly related by Eq. (8). Dots denote the unstrained structure.

change in the orbital occupancy as a function of strain. As discussed earlier, the Q_3 mode is directly related linearly to ε_{zz} through Eq. (8). Quite interestingly, we find that the magnitude of the in-plane distortion Q_2 at first diminishes and then sharply drops to zero as the strain is changed from compressive to tensile. This is due to the fact that in the compressive strain condition, the system stabilizes in the type G AFM ordering where the Q_2 mode is more favorable (see Fig. 6). On the other hand, in the tensile strain condition, in the stable ferromagnetic (F) ordering, kinetic-energy gain is maximum if the e_g orbitals are not split, so that the JT distortion is small or nonexistent.

Strain has a strong effect on the e_g orbital occupancies as indicated in Fig. 7. The calculated orbital occupancies are plotted in Fig. 10. In the A phase, the x^2-y^2 and the z^2-1 orbitals add up with the proper linear combination to yield the checkerboard x^2-1/y^2-1 orbital ordering on alternate Mn atoms in the ab plane. As the strain is increased, the z^2-1 orbital becomes more and more occupied with the occupancy becoming one in the G′ phase. This is because in this limit Q_3 is large and Q_2 is zero, so that the elongated Mn-O bond along the c axis results in a strong octahedral crystal field that increases the energy of x^2-y^2 orbital, simultaneously lowering that of z^2-1 orbital and fully occupying it in the process. This physics is of course incorporated in the linear Jahn-Teller coupling term in our model Hamiltonian Eq. (3).

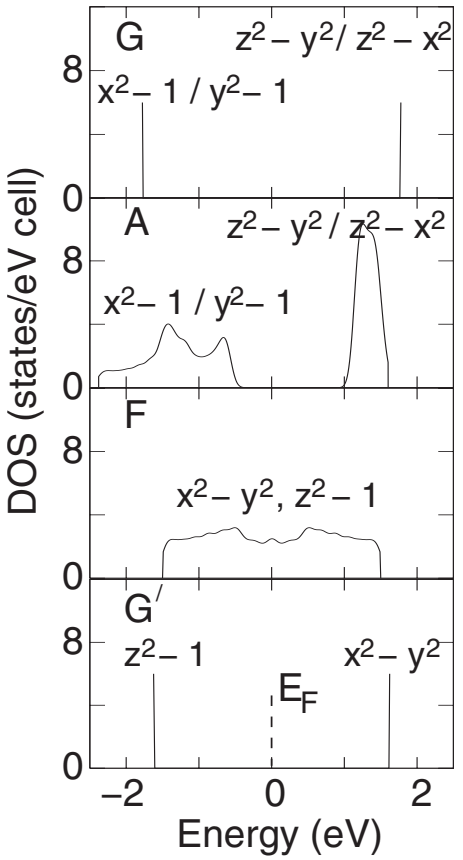

FIG. 11. DOSs corresponding to the four strain conditions of Fig. 2. In the Néel ordered G and G′ phases, complete suppression of hopping leads to the δ functions in the DOS. In the G phase, alternate Mn sites have the x^2-1 or the y^2-1 orbitals occupied with the remaining component of the e_g manifold empty, leading to the checkerboard orbital ordering, while in the G′ phase, all sites have the z^2-1 orbital occupied. In the A phase, allowed hopping in the plane leads to a broadening of the band, but still a gap in the DOS remains. In the ferromagnetic F phase, hopping both in and out of the plane is strong enough to close the gap, leading to a metallic state due to band gap closure. The second set of parameters was used to calculate this figure and the Fermi energy is taken as the zero of energy.

Beside the magnetic transitions, the other important feature in the strain induced LMO is a metal-insulator transition due to band gap closure. Figure 11 shows the densities of states (DOSs) for the various phases, which faithfully indicates the strong JT splitting of the on-site energies of the e_g orbitals, $\Delta=2g\sqrt{Q_2^2+Q_3^2}$, with only a large hopping in the ferromagnetic phase being able to close the gap and produce a metallic phase. In Fig. 12, we have shown the calculated band gap as a function of strain. We see that the gap changes abruptly as new phases are entered. We note that for the unstrained case, the magnitude of the band gap obtained with our parameters is 1.85 eV as compared to the measured value of 1.8 eV, obtained from the photoemission data.[42] This suggests that the experimental band gap under strain may also show changes similar to what is indicated from our model. Again the trends in the calculated band gaps are the same for the two parameter sets, with and without U.

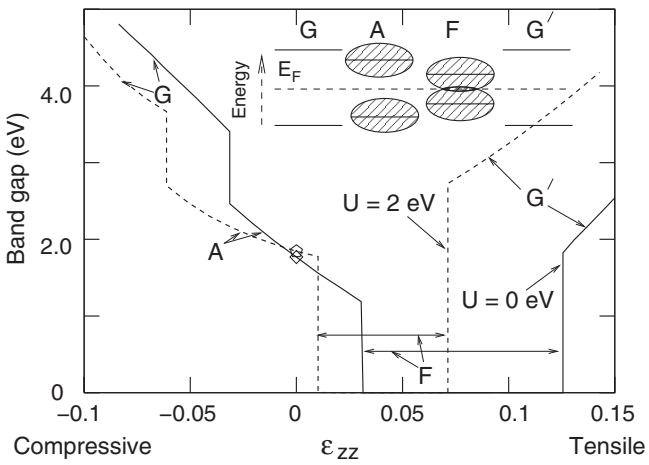

FIG. 12. Variation in the band gap with strain. Inset shows the typical band structure for the four phases. Diamonds indicate the band gap for the unstrained LMO. Results are shown for two sets of parameters corresponding to with and without a Coulomb interaction term.

IV. SUMMARY

In summary, we studied the effect of uniaxial strain on the ground-state structure of $LaMnO_3$ from a model Hamiltonian that included the key interactions in the system, viz., the superexchange, the double exchange, and the Jahn-Teller electron-lattice coupling. Inclusion of an on-site Coulomb interaction term does not alter the basic results obtained from the model. Our results reveal the existence of various phases under varying strain conditions, where the orbital order, magnetic structure, octahedral JT distortions, as well as the conduction properties change under applied strain. Only the ferromagnetic phase, stable with a small tensile strain in our model, was found to be metallic, while all other phases were found to be insulating. The analysis presented here should be helpful in the interpretation of experiments on epitaxially grown $LaMnO_3$ heterostructures, which are often in the uniaxial strain condition.

ACKNOWLEDGMENT

This work was supported by the U. S. Department of Energy through Grant No. DE-FG02-00ER45818.

[1] C. Christides, P. P. Deen, N. Moutis, E. Houssakou, L. Bouchenoire, and K. Prassides, Phys. Rev. B **75**, 014432 (2007).
[2] H. Yamada, M. Kawasaki, T. Lottermoser, T. Arima, and Y. Tokura, Appl. Phys. Lett. **89**, 052506 (2006).
[3] T. Koida, M. Lippmaa, T. Fukumura, K. Itaka, Y. Matsumoto, M. Kawasaki, and H. Koinuma, Phys. Rev. B **66**, 144418 (2002).
[4] T. Satoh, K. Miyano, Y. Ogimoto, H. Tamaru, and S. Ishihara, Phys. Rev. B **72**, 224403 (2005).
[5] Ş. Smadici, P. Abbamonte, A. Bhattacharya, X. Zhai, B. Jiang, A. Rusydi, J. N. Eckstein, S. D. Bader, and J. M. Zuo, Phys. Rev. Lett. **99**, 196404 (2007).
[6] B. R. K. Nanda and S. Satpathy, Phys. Rev. Lett. **101**, 127201 (2008).
[7] A. Y. Ramos, H. C. N. Tolentino, N. M. Souza-Neto, J.-P. Itié, L. Morales, and A. Caneiro, Phys. Rev. B **75**, 052103 (2007).
[8] I. Loa, P. Adler, A. Grzechnik, K. Syassen, U. Schwarz, M. Hanfland, G. Kh. Rozenberg, P. Gorodetsky, and M. P. Pasternak, Phys. Rev. Lett. **87**, 125501 (2001).
[9] L. Pinsard-Gaudart, J. Rodriguez-Carvajal, A. Daoud-Aladine, I. Goncharenko, M. Medarde, R. I. Smith, and A. Revcolevschi, Phys. Rev. B **64**, 064426 (2001).
[10] Y. Ding, D. Haskel, Y.-C. Tseng, E. Kaneshita, M. van Veenendaal, J. F. Mitchell, S. V. Sinogeikin, V. Prakapenka, and H. K. Mao, Phys. Rev. Lett. **102**, 237201 (2009).
[11] A. Tebano, C. Aruta, S. Sanna, P. G. Medaglia, G. Balestrino, A. A. Sidorenko, R. De Renzi, G. Ghiringhelli, L. Braicovich, V. Bisogni, and N. B. Brookes, Phys. Rev. Lett. **100**, 137401 (2008); C. Aruta, G. Ghiringhelli, A. Tebano, N. G. Boggio, N. B. Brookes, P. G. Medaglia, and G. Balestrino, Phys. Rev. B **73**, 235121 (2006); A. Tebano, A. Orsini, P. G. Medaglia, and G. Balestrino, Appl. Phys. Lett. **94**, 242503 (2009).
[12] Y. Konishi, Z. Fang, M. Izumi, T. Manako, M. Kasai, H. Kuwahara, M. Kawasaki, K. Terakura, and Y. Tokura, J. Phys. Soc. Jpn. **68**, 3790 (1999).
[13] J. Zhang, H. Tanaka, T. Kanki, J.-H. Choi, and T. Kawai, Phys. Rev. B **64**, 184404 (2001).
[14] J. H. Song, J. H. Park, K.-B. Lee, J. M. Lee, and Y. H. Jeong, Phys. Rev. B **66**, 020407(R) (2002).
[15] A. Dubey, V. G. Sathe, and R. Rawat, J. Appl. Phys. **104**, 113530 (2008).
[16] Y. Suzuki, H. Y. Hwang, S.-W. Cheong, and R. B. van Dover, Appl. Phys. Lett. **71**, 140 (1997).
[17] J. Z. Sun, D. W. Abraham, R. A. Rao, and C. B. Eom, Appl. Phys. Lett. **74**, 3017 (1999).
[18] H. Meskine, H. König, and S. Satpathy, Phys. Rev. B **64**, 094433 (2001).
[19] B. R. K. Nanda and S. Satpathy, Phys. Rev. B **79**, 054428 (2009).
[20] B. R. K. Nanda and S. Satpathy, Phys. Rev. B **78**, 054427 (2008).
[21] S. Satpathy, Z. S. Popović, and F. R. Vukajlović, Phys. Rev. Lett. **76**, 960 (1996).
[22] D. J. Singh and W. E. Pickett, Phys. Rev. B **57**, 88 (1998).
[23] W. E. Pickett and D. J. Singh, Phys. Rev. B **53**, 1146 (1996).
[24] H. Zenia, G. A. Gehring, and W. M. Temmerman, New J. Phys. **7**, 257 (2005).
[25] G. Trimarchi and N. Binggeli, Phys. Rev. B **71**, 035101 (2005).
[26] A. Yamasaki, M. Feldbacher, Y.-F. Yang, O. K. Andersen, and K. Held, Phys. Rev. Lett. **96**, 166401 (2006).
[27] B. R. K. Nanda and S. Satpathy (unpublished).
[28] J. Kanamori, J. Appl. Phys. **31**, S14 (1960).
[29] Z. Popović and S. Satpathy, Phys. Rev. Lett. **84**, 1603 (2000).
[30] C. Zener, Phys. Rev. **82**, 403 (1951).
[31] P. W. Anderson and H. Hasegawa, Phys. Rev. **100**, 675 (1955).
[32] W. A. Harrison, *Electronic Structure and the Properties of Solids* (Freeman, San Francisco, 1979).
[33] A. J. Millis, Phys. Rev. B **53**, 8434 (1996).
[34] E. O. Wollan and W. C. Koehler, Phys. Rev. **100**, 545 (1955).
[35] G. S. Rushbroke, G. S. Baker, Jr., and P. J. Wood, in *Phase Transitions and Critical Phenomena*, edited by C. Domb and M. S. Green (Academic Press, London, New York, 1974), Vol. 3, Eqs. (1.1) and (5.4).
[36] I. Solovyev, N. Hamada, and K. Terakura, Phys. Rev. B **53**, 7158 (1996).
[37] P. Benedetti and R. Zeyher, Phys. Rev. B **59**, 9923 (1999).
[38] J. B. A. A. Elemans, B. van Laar, K. R. van der Veen, and B. O. Loopstra, J. Solid State Chem. **3**, 238 (1971).
[39] C. Adamo, X. Ke, H. Q. Wang, H. L. Xin, T. Heeg, M. E. Hawley, W. Zander, J. Schubert, P. Schiffer, D. A. Muller, L. Maritato, and D. G. Scholm, Appl. Phys. Lett. **95**, 112504 (2009).
[40] H. R. Salva, A. A. Ghilarducci, A. G. Leyva, and S. S. Seiro, J. Magn. Magn. Mater. **310**, e626 (2007).
[41] I. B. Bersuker, *The Jahn-Teller Effect and Vibronic Interactions in Modern Chemistry* (Plenum Press, New York, 1984).
[42] T. E. Saitoh, A. E. Bocquet, T. Mizokawa, H. Namatame, A. Fujimori, M. Abbate, Y. Takeda, and M. Takano, Phys. Rev. B **51**, 13942 (1995).